ACS Chemical Neuroscience

pubs.acs.org/chemneuro Research Article

Synthesis and Characterization of a Diazirine-Based Photolabel of the Nonanesthetic Fropofol

E. Railey White, David M. Leace, Victoria M. Bedell, Natarajan V. Bhanu, Benjamin A. Garcia, William P. Dailey, and Roderic G. Eckenhoff*

Cite This: *ACS Chem. Neurosci.* 2021, 12, 176–183 Read Online

ACCESS | Metrics & More | Article Recommendations | Supporting Information

ABSTRACT: The mechanisms of general anesthetics have been debated in the literature for many years and continue to be of great interest. As anesthetic molecules are notoriously difficult to study due to their low binding affinities and multitude of binding partners, it is advantageous to have additional tools to study these interactions. Fropofol is a hydroxyl to fluorine-substituted propofol analogue that is able to antagonize the actions of propofol. Understanding fropofol's ability to antagonize propofol would facilitate further characterization of the binding interactions of propofol that may contribute to its anesthetic actions. However, the study of fropofol's molecular interactions has many of the same difficulties as its parent compound. Here, we present the synthesis and characterization of *ortho*-azi-fropofol (AziF*o*) as a suitable photoaffinity label (PAL) of fropofol that can be used to covalently label proteins of interest to characterize fropofol's binding interactions and their contribution to general anesthetic antagonism.

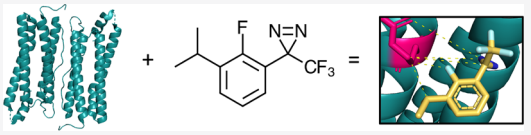

KEYWORDS: *Anesthetic antagonist, propofol, molecular probe, photoaffinity label, hydrogen bonding, fluorine*

INTRODUCTION

The introduction of propofol (2,6-diisopropylphenol) in the late 1980s marked the first alkylphenol anesthetic agent to be used in anesthetic practice.[1] This molecule remains structurally unique compared to other general anesthetic agents and has become one of the most frequently used medications in the practice of anesthesia.[2] Many studies have explored the medicinal chemistry of alkylphenol anesthetics and have worked to define the chemical space that they inhabit.[3−6] Seemingly subtle structural changes occasionally result in the complete elimination of anesthetic activity, but the loss of hypnotic or sedating activity does not necessarily render these compounds biologically inactive. One such molecule that was initially thought to be "inactive" is a fluorinated analogue of propofol (fropofol) where a fluorine has been substituted for the hydroxyl group (Figure 1).[7] This loss of hydrogen bonding character abrogates any sedative/hypnotic activity and exhibits an excitatory phenotype at high doses (200 mg/kg in mice).[7] At concentrations much lower than necessary to generate this excitation, fropofol is able to antagonize the sedative effect of propofol.[7] The mechanism of this antagonism is not fully understood, but there are data to support that fropofol does not modulate the $\alpha1\beta2\gamma2$L isoform of $GABA_A$, making a GABAergic mechanism less likely than another as yet unidentified molecular target.[7]

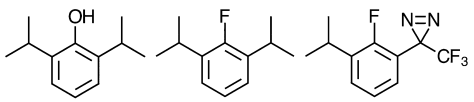

Propofol Fropofol *ortho*-Azi-Fropofol (AziF*o*, **1**)

Figure 1. Chemical structures. Shown are the structures of the anesthetic propofol, its fluorine-substituted derivative, fropofol, and the diazirine-based photolabel of fropofol, *ortho*-azi-fropofol (AziF*o*, **1**).

Due to the structural similarity of fropofol to propofol and their seemingly opposite pharmacologic effects, fropofol could prove a useful tool in probing the anesthetic mechanism of propofol, which remains an area of significant interest.[8,9] As small hydrophobic molecules, anesthetics have been notoriously difficult to study due to their relatively low binding affinities at a large number of target sites. These hurdles have previously been overcome in part by developing diazirine-based photoaffinity labels (PALs) of the molecules of interest.[10] The incorporation of a diazirine moiety allows the formation of nonspecific covalent bonds through a reactive carbene intermediate formed in the presence of UV light.[11,12] By irreversibly linking the PAL to the macromolecule of interest, a snapshot of a low-affinity, transient interaction can be studied in detail.[10] Fropofol, like propofol and most other anesthetics, is a small molecule (MW = 246.21 amu), and it is well established that making seemingly minor changes to these

Received: October 16, 2020
Accepted: December 8, 2020
Published: December 23, 2020

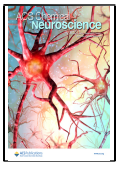

https://dx.doi.org/10.1021/acschemneuro.0c00667
ACS Chem. Neurosci. 2021, 12, 176−183

Scheme 1. Synthesis of AziFo (1)

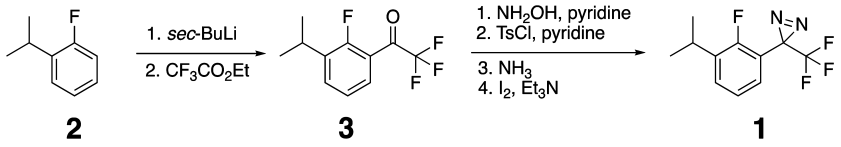

drugs can have a significant impact on their function.[3−6] Thus, before a photolabel can be deployed to study the molecular actions of its parent compound, it is critical to establish that the substitution of the isopropyl group for a diazirine results in comparable activity.[13,14] Without assuring a similar function, a PAL will fail to be an adequate surrogate of its parent compound. Here, we describe the synthesis of *ortho*-azi-fropofol (AziFo) and its characterization as a suitable PAL of fropofol.

RESULTS AND DISCUSSION

Synthesis of Azi-fropofol (1). The proposed PAL analog of fropofol presented here is 3-(2-fluoro-3-isopropylphenyl)-3-(trifluoromethyl)-3*H*-diazirine (*ortho*-azi-fropofol, AziFo **1**, Figure 1). Compared with fropofol, AziFo replaces one of the isopropyl groups on the aromatic ring with the photoreactive trifluoromethyl diazirine groups. The synthesis of AziFo (Scheme 1) involved the conversion of 1-fluoro-2-isopropylbenzene to the known trifluoromethyl ketone **3**.[15] The conversion of ketone **3** to the corresponding diazirine **1** followed well-established protocols.[16] Azi-fropofol (**1**) was obtained as a liquid in >98% purity as measured by capillary GC.

Physiochemical Characterization. The first step in establishing the suitability of AziFo as a PAL of fropofol was to compare physiochemical properties, which are shown in Table 1. When compared to fropofol, AziFo has a 36% increase in molecular weight but does not have a proportional increase in van der Waals volume. Therefore, it is no surprise that AziFo has a higher density of 1.2 g/cm^3 compared to fropofol's density of 0.9 g/cm^3. This increase corresponds to general trends in the fluorination of hydrocarbons.[17] The calculation of the octanol/water partition coefficient (cLogP) indicates a marginal increase in the hydrophobicity of AziFo (cLogP of 4.14) compared to fropofol (cLogP of 3.96), which correlates to their relative maximal water solubility (95 and 116 μM, respectively).

Table 1. Physiochemical Properties of Fropofol and AziFo

physiochemical properties	fropofol[a]	azi-fropofol (AziFo)
molecular weight (amu)	180.26	246.21
van der Waals volume (Å^3)	189	195
density (g/cm^3; mean ± SD)	0.9	1.19 ± 0.01
cLogP[b]	3.96	4.14
solubility in water (μM; mean ± SD)	116 ± 4	95 ± 4

[a]All fropofol data are values that have been previously reported.[18] [b]cLogP = octanol/water partition coefficient.

Fluorescence Competition with Horse Spleen Apoferritin. 1-Aminoanthracene (1-AMA) exhibits enhanced fluorescence when bound to horse spleen apoferritin (HSAF). Fropofol and AziFo are both able to displace 1-AMA from its known binding pocket in HSAF. This competition assay with fropofol and AziFo yielded IC_{50} values for fropofol and AziFo of 11 and 17 μM, respectively (Figure 2). Utilizing these values and an experimentally determined binding affinity of 1-AMA and HSAF (9 μM) (Figure S9), the Cheng-Prusoff equation was used to calculate K_D values, which were 4.3 μM (95% CI of 3.1−5.7) for fropofol and 6.6 μM (95% CI of 4.7−11.7) for AziFo.[18]

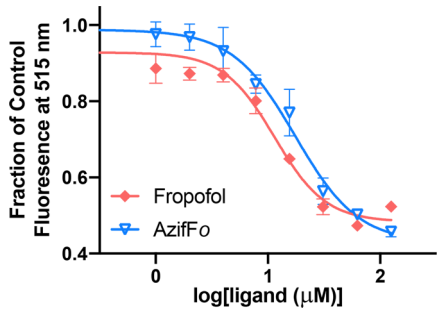

Figure 2. 1-AMA competition assay. HSAF binding affinities of AziFo and fropofol were calculated from their displacement of the known binding partner 1-AMA, which exhibits increased fluorescence when bound to HSAF.

Activity of AziFo in Zebrafish. Zebrafish (*Danio rerio*) larvae at 5 days postfertilization (dpf) were initially exposed to concentrations as high as 100 μM AziFo or fropofol for 30 min. No decrease in spontaneous movement was observed, and no increases in activity or alterations in swimming pattern that may be consistent with an excitatory or seizure phenotype were observed. After these responses were noted, larvae were then transferred to fresh zebrafish embryo water (E3) and observed for 24 h after which 3 of 12 larvae in the 100 μM fropofol exposure were found dead. No toxicity was seen during tests of up to 100 μM AziFo, and concentrations no higher than 25 μM were used for either compound in the subsequent experiments. Because of the seemingly absent pharmacologic effect of both ligands, AziFo and fropofol (at 5 or 25 μM) were coadministered with propofol (0.03−10 μM) to look for pharmacologic additivity. Instead of additivity, both AziFo and fropofol showed a dose-dependent antagonism of propofol-induced hypnosis as measured by a decrease in spontaneous movement (Figure 3).[19]

AziFo Diazirine Half-Life. The UV−vis absorption spectrum of AziFo showed a local maximum from the diazirine at 317 nm with additional aromatic absorbance maxima at 273 and 267 nm (Figure S7). An experimentally determined extinction coefficient of 1600 M^{-1} cm^{-1} at 273 nm was used for all determinations of concentration based on the absorption. The signal at 317 nm was of insufficient intensity to be useful at working concentrations in aqueous solutions; thus, the half-life of the AziFo diazirine was determined in methanol to overcome the limitation in solubility. Upon exposure to 356 nm light, the half-life ($t_{1/2}$) of the diazirine peak (317 nm) was 11.0 min (95% CI of 6.6−26.5) (Figure 4). Degradation after a 300 nm exposure was faster with a $t_{1/2}$ of

https://dx.doi.org/10.1021/acschemneuro.0c00667
ACS Chem. Neurosci. 2021, 12, 176−183

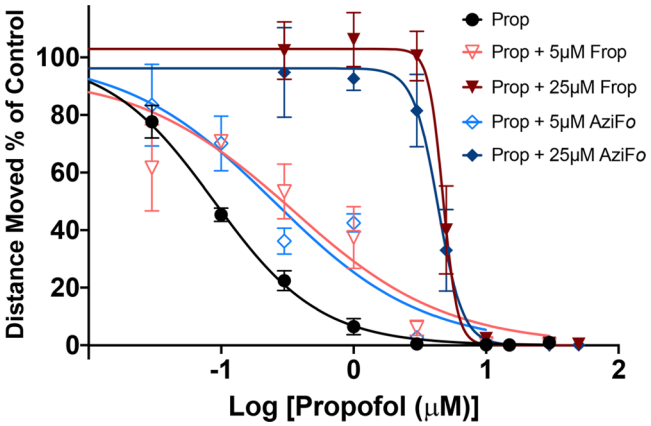

Figure 3. Activity of AziF*o* in vivo. No change (neither decrease nor increase) in spontaneous movement was observed upon exposure of 5 dpf zebrafish to maximal nontoxic doses of AziF*o* or fropofol. The administration of propofol (Prop) alone demonstrates a dose-dependent decrease in spontaneous movement. Shown here is the effect of coadministration of AziF*o* or fropofol (Frop) with propofol, and the resultant dose-dependent antagonism of propofol's effects (5 and 25 μM doses shown). Data for propofol alone has been previously published.[19]

3.8 min (95% CI of 2.9−4.8) (Figure 4). The exposure to a 300 nm light was used for all photolabeling experiments.

Photoadduction to HSAF. After irradiating a solution of 10 μM AziF*o* and HSAF with a 300 nm UV light for 25 min, trypsinization, and analysis by LC/MS/MS, 98.3% sequence coverage of the HSAF light chain sequence was detected, and MaxQuant was used to search for AziF*o* adducts (+218.0719 m/z). At a 10 μM AziF*o* concentration, there was only one potential photolabeled site detected. This site was in the middle of a peptide 34 amino acids in length (Figures S12 and S13), so it is not surprising that there was insufficient spectral data to identify the labeling of a specific amino acid within this sequence. However, it was somewhat promising that portions of this suspected labeling site fall within the known ligand binding site of HSAF, which was previously photolabeled with AziP*m* (*meta*-azi-propofol), a propofol PAL.[13] An additional photolabeling reaction was conducted with 100 μM AziF*o*. From this reaction, protein sequence coverage was 78.7% (Figure S11) and there were 3 possible photoadduction sites identified (Arg-59, Met-144, and Gln-82). The labeled Gln-82 was only seen in <2% of spectra that identified its peptide sequence, and the labeled Met-144 was seen in 12% of spectra that identified its peptide sequence (for the best spectra, see Figures S14 and S15). This low frequency of labeling, combined with the overall poor-quality MS/MS spectra, makes these more likely to be nonspecific labeling sites. On the other hand, the labeling of Arg-59 with AziF*o* was seen in over half of the MS/MS sample spectra that identified the peptide sequence that contained this site (ELAEEK$\mathbf{R}_{59}$-EGAER) and had overall higher quality MS/MS spectra (Figure S16), which makes it much more likely to be a photoadduction site representative of a meaningful interaction of HSAF and AziF*o*.

Given that no photoadduction sites were identified at 10 μM AziF*o* and there were some possible nonspecific labeling sites identified at 100 μM AziF*o*, an additional round of photolabeling was conducted with an intermediate concentration of AziF*o* (50 μM). This intermediate concentration only supported one photolabeled site, again showing strong evidence for the same Arg-59 site identified in the 100 μM photolabeling experiment (Figure 5). There was also some weak evidence for a second possible biding site between Asn-17 and Leu-31 in the middle of the same 34 amino acid length peptide previously identified (Figure S17). This peptide is the product of two missed trypsin cleavages, and the "blind spot" peptide was identified this time and included a photolabeled site. The spectrum of this peptide (LVNLYLR) (Figure S18) identified Leu2-4 as the labeled site; however, there was only a single spectrum at low intensity.

Both Leu-24 and Arg-59 of HSAF have been shown to be among the amino acids to demonstrate specific noncovalent interactions with propofol and fropofol,[20,21] and Leu-24 was the photolabeled site previously identified with the propofol analogue AziP*m*.[13] The evidence presented here only strongly supports an Arg-59 site, despite many other residues that line the known "anesthetic" pocket of HSAF. These residues of this pocket can be seen in a CASTp analysis (Figure S19). Each of these residues have been previously identified via computational modeling and the propofol bound crystal structure of HSAF.[20,21]

In providing an answer to which amino acids are photolabeled, it is important to consider the questions we posed by performing a photolabeling experiment with AziF*o* vs AziP*m*. It is reasonable to think that the preference for AziF*o* to label Arg-59, rather than Leu-24, is due to differences in the pose that AziP*m* and AziF*o* assume in the HSAF site. For example, a significant determinant of adduct formation is the position of the reactive carbene derived from the diazirine arm relative to the lining residues. For AziF*o* and AziP*m*, this arm is

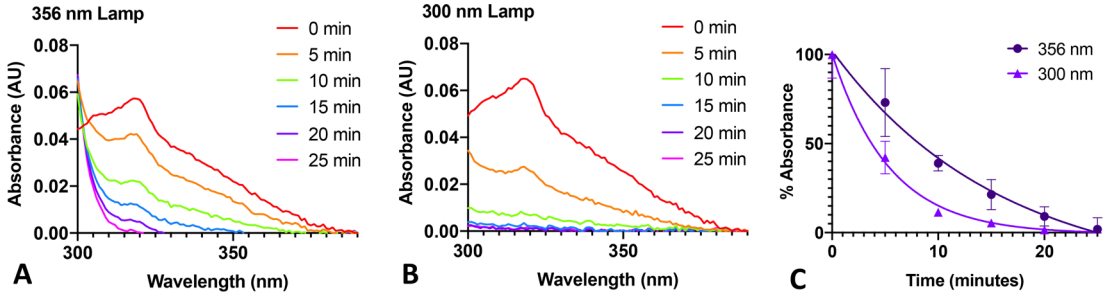

Figure 4. Determination of diazirine half-life. The disappearance of the diazirine upon exposure to UV light was monitored via UV−vis absorption. (A) UV−vis spectra during exposure to 356 nm light. (B) UV−vis spectra during exposure to 300 nm light. (C) Graphical representation of absorption vs time showing the relative difference in diazirine degradation kinetics between the two exposure wavelengths. Absorbance was measured at 317 nm.

https://dx.doi.org/10.1021/acschemneuro.0c00667
ACS Chem. Neurosci. 2021, 12, 176−183

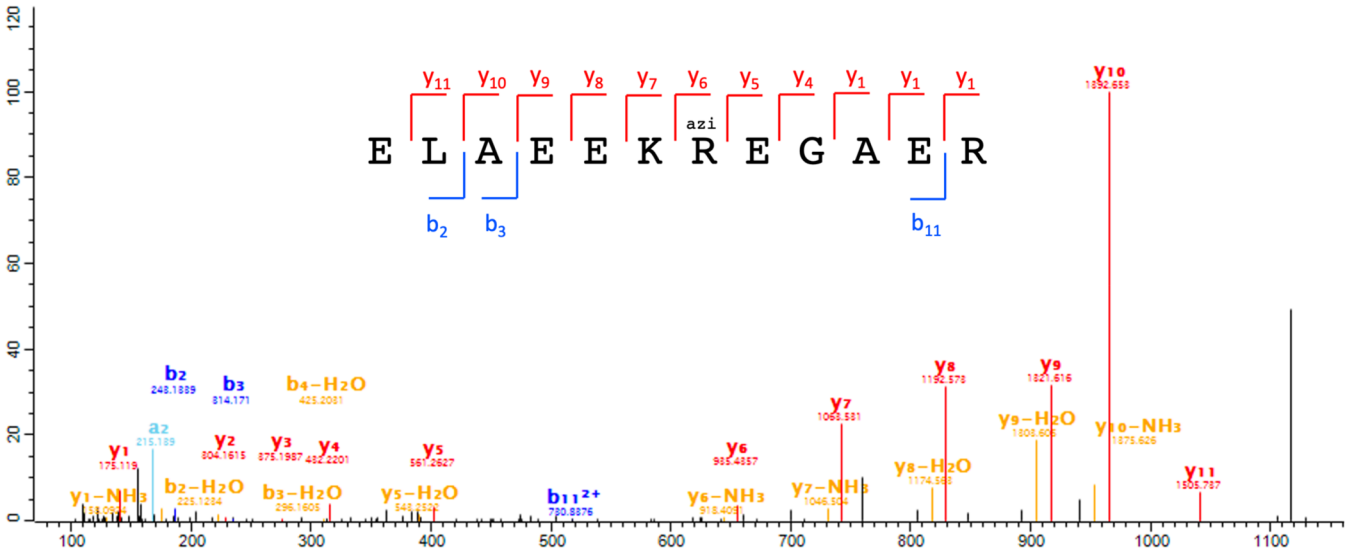

Figure 5. MS/MS spectrum of AziF*o* adduction to R59. MS/MS fragmentation spectrum of the peptide ELAEEKREGAER (amino acids 53 to 64), which contains the Arg identified as a site photolabeled by AziF*o* (50 μM). Fragments identified on the spectrum are shown on the peptide sequence (b ions in blue; y ions in red). A detailed ion table can be found in Table S6.

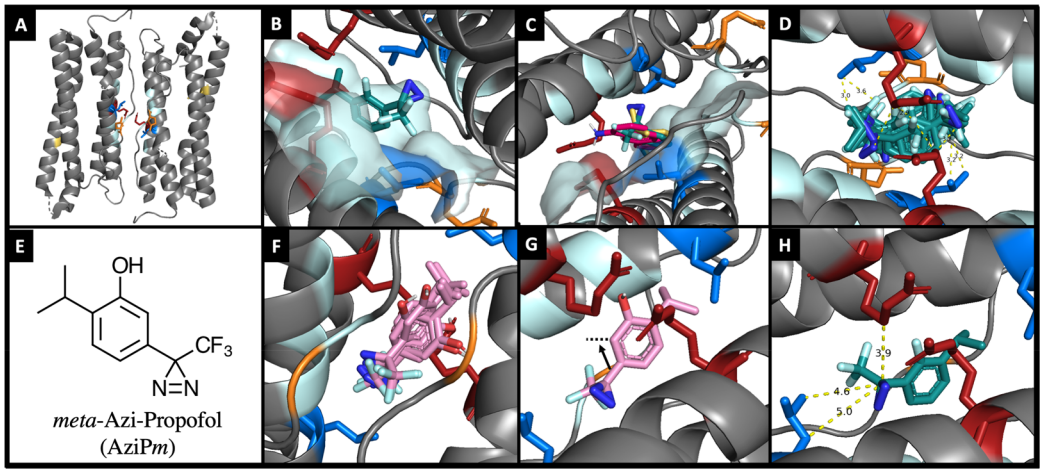

Figure 6. Visualization of AziF*o* and photolabeled residues. Utilizing a previously reported crystal structure (PDB ID 3f32), docking calculations using AutoDock Vina were conducted to analyze the relationship between possible ligand confirmations and the photolabeled Arg-59. (A) HSAF dimer (gray) with the location of possible photolabeled adducts (red = Arg-59, blue = Leu-24, orange = Gln-82, and yellow = Met-144) and the location of the amino acids known to line the ligand binding pocket (light green, Ser-27, Tyr-28, Glu-63, and Leu-81). (B) Demonstration of lowest energy AziF*o* docking pose within the ligand binding pocket (dark green = carbon, light green = fluorine, and blue = diazirine nitrogens). (C) Lowest energy docking pose for 1-AMA (bright pink), fropofol (yellow), and AziFo (teal) within the ligand binding pocket. (D) All docking poses of AziF*o*. The closest distance of any atom of any AziF*o* confirmation to the nearest Arg-59 atom was 2.9 Å. (E) The chemical structure of *meta*-Azi-Propofol (AziP*m*). Note the *meta* position of the diazirine arm compared to the *ortho* position of AziFo (Figure 1). (F) Docking poses 2, 3, 5, 7, and 9 of AziP*m* with the diazirine group oriented toward one of the two Leu-24. Poses 1, 4, 6, and 8 were of approximately the opposite symmetry with the diazirine arm oriented toward the other Leu-24. (G) A single AziP*m* pose indicating the difference in position between the *meta* diazirine arm of AziP*m* and the *ortho* position of AziF*o*. Arrow and dotted line indicate the theoretical movement of the arm to the *ortho* position. (H) A single pose of AziF*o* showing a closer proximity of the diazirine carbon to Arg-59 (red) than Leu-24 (light green). Measurements are in angstroms.

in different positions on the aromatic ring (*ortho* vs *meta* with respect to the fluorine/hydroxyl). Because of these differences in geometry, it is not entirely surprising that these PALs result in different binding sites. In fact, in the crystal structure of propofol bound to HSAF, the isopropyl arms are packed against the hydrophobic portions of both Arg-59 side chains.[21] Given the fact that AziF*o* has a direct substitution of an isopropyl arm for a diazirine arm, it is not surprising that this close interaction results in selective photolabeling of this residue. This change in orientation can be more easily seen by docking AziF*o* within the HSAF pocket (Figure 6).

Molecular Docking Calculations. To demonstrate the occupation of AziF*o* in the known ligand binding site of HSAF, molecular docking calculations were conducted with AutoDock Vina.[22] This model helps to provide a visual representation and approximate measurement of atomic distances between the docked PAL and protein crystal structure. The ligand binding pocket is formed at the interface of HSAF homodimers and is lined by 6 amino acids (L24, S27, Y28, R59, E63, and L81; see Figures 6A and S19). The symmetry of this dimerization puts the Arg-59 from both proteins in close proximity within the ligand binding pocket

https://dx.doi.org/10.1021/acschemneuro.0c00667
ACS Chem. Neurosci. 2021, 12, 176−183

(Figure 6A). The lowest energy poses of AziFo, fropofol, and 1-AMA can be seen in Figure 6B,C. Even with this simple docking model, AziFo shows a preference of position within the pocket. It is easiest to see the clustering of the diazirine nitrogens, which are oriented in proximity to Arg-59 and Leu-24 (Figure 6D).

To compare how AziPm and AziFo might bind in the HSAF pocket, docking simulations were also conducted with AziPm (Figure 6E). Consistent with AziFo docking, AziPm showed a clustering of the diazirine groups in proximity to Leu-24 and Arg-59 (Figure 6F), but there is an important difference in the position of the diazirine arm. It is known from the crystal structure of ligands bound to HSAF that the propofol hydroxl prefers to face the opening of the pocket (toward the two arginines). If this orientation is preserved, then the position of the diazirine arm becomes an important predictor of what residues are photolabeled by each ligand. Figure 6G shows AziPm with the diazirine arm oriented toward Leu-24 (shown in blue). If one imagines the theoretical repositioning of that arm to an *ortho* position (dotted line in Figure 6G), then the arm moves into closer proximity of Arg-59. Figure 6H shows a single pose of AziFo and the relative closeness of Arg-59 (red) and Leu-24 (blue). It should be noted that the measurements shown in Figure 6 are the closest distances that were found; there is no way of knowing exactly to which atom on the arginine (including the backbone) the PAL adducted.

During docking calculations, the backbone is rigid and the side chains are allowed to move. Therefore, comparisons made between a previously determined crystal structure and a docking calculation with a novel ligand may not be a reliable representation of binding conditions. Despite these limitations, the structural relationships support the photoadduction site identified by MS/MS sequencing as a realistic target of the AziFo PAL and may help to explain the difference in selectivity between AziFo and AziPm.

CONCLUSION

In order to determine if AziFo closely mimics its parent compound fropofol and is viable as a PAL, we compared physiochemical properties, interactions with a model protein, and pharmacologic activity in zebrafish. When combined with the ability of AziFo to successfully adduct HSAF, this data serves to support the use of AziFo as a surrogate molecule for further study of the mechanism of action of fropofol. A single amino acid (Arg-59) in HSAF was identified as a photolabeled site within the known binding pocket. In addition to the MS/MS data, AziFo's ability to displace 1-AMA provides additional evidence that this site is specific and not the result of random off-site labeling. Specificity is a necessary trait for deploying AziFo into more complex biological systems of interest. The functional similarity of fropofol and AziFo combined with the ability of AziFo to successfully adduct a known fropofol binding site of HSAF serves to support the use of AziFo as a surrogate molecule for further study of the mechanism of action of fropofol.

One plausible explanation of fropofol's inhibition of propofol's action is simply that it is binding in the same "anesthetic" site(s). This would support the notion that the mere occupancy of a site is insufficient to generate anesthesia. The character of the molecule and the interactions it makes within the site may have important and even opposing effects on pharmacodynamics. However, at this point in time, we have not ruled out the possibility of entirely different binding sites and different molecular targets.

Like many approaches, AziFo is only one of many tools in the toolbox needed to understand anesthetic mechanisms. It can provide a starting point for subsequent, complementary experimental and computational methods.

METHODS

General Synthetic Procedures. Proton and ^{13}C NMR spectra were obtained on a Bruker DMX 500 MHz nuclear magnetic resonance spectrometer, and ^{19}F NMR spectra were obtained on a Bruker DMX 360 MHz nuclear magnetic resonance spectrometer. Spectra for compounds **1** and **3** are reported in the Supporting Information. Accurate mass measurement analyses were conducted on either a Waters GCT Premier, time-of-flight GCMS with electron ionization (EI) or an LCT Premier XE, time-of-flight LCMS with electrospray ionization (ESI). Samples were taken up in a suitable solvent for analysis. The signals were mass measured against an internal lock mass reference of perfluorotributylamine (PFTBA) for EI-GCMS and leucine enkephalin for ESI-LCMS. Waters Masslynx software calibrates the instruments and reports measurements by the use of neutral atomic masses. The mass of the electron is not included.

Preparation of 2,2,2-Trifluoro-1-(2-fluoro-3-isopropylphenyl)ethan-1-one (3). A 250 mL round-bottom flask equipped with a magnetic stirring bar was filled with 100 mL of dry THF and 2.76 g (20 mmol) of 1-fluoro-2-isopropylbenzene. Under a dry nitrogen atmosphere, the clear, colorless solution was cooled in a dry ice/acetone bath with stirring for 30 min. A solution of 1.3 M *sec*-BuLi in cyclohexane (18.0 mL, 23 mmol) was added dropwise over the course of 10 min. The solution was stirred for an additional 10 min at dry ice temperature. Ethyl trifluoroacetate (4.0 mL, 4.8 g, 34 mmol) was added dropwise over 10 min to the cooled, stirred solution. After stirring an additional 10 min in the cold bath, the solution was allowed to warm to room temperature and was quenched with 100 mL of 10% hydrochloric acid (HCl) solution. The mixture was extracted with methylene chloride (3 × 100 mL). The combined organic extracts were washed with water, and the dried organic layer was evaporated. Short-path distillation of the residue under reduced pressure produced 3.43 g (73%) of clear, colorless oil, bp 108−109 °C at 25 mmHg. ^1H NMR (500 MHz, $CDCl_3$) δ 7.69 (t, J = 7.1, 1H), 7.60 (td, J = 7.1, 1.8 Hz, 1H), 7.25 (t, J = 7.8 Hz, 1H), 3.33 (p, J = 6.9 Hz, 1H), 1.29 (dd, J = 7.0, 2.4 Hz, 6H). ^{19}F-NMR (340 MHz, $CDCl_3$) −74.43 (d, J = 15.7 Hz, 3F), −114.97 (td, J = 15.7, 6.8 Hz, 1F) ppm. ^{13}C NMR (90 MHz, $CDCl_3$) 179.80 (q, J = 38 Hz), 159.8 (d, J = 261 Hz), 137.3 (d, J = 15 Hz), 134.3 (d, J = 7 Hz), 128.8, 124.5 (d, J = 4 Hz), 119.7 (d, J = 11 Hz), 116.0 (q, J = 291 Hz), 27.0 (d, J = 3 Hz), 22.4 ppm. HRMS (EI+) calculated for $C_{11}H_{11}F_4O$ $[M + H]^+$: 235.0746, found: 235.0753.

Preparation of 3-(2-Fluoro-3-isopropylphenyl)-3-(trifluoromethyl)-3*H*-diazirine (Azi-fropofol) (1). A 100 mL round-bottom flask equipped with a magnetic stirrer was filled with 3.00 g (12.8 mmol) of ketone **3**, 1.00 g (14.5 mmol) of hydroxylamine hydrochloride, and 50 mL of pyridine. A water-cooled reflux condenser was attached, and the mixture was heated to reflux for 1 h. After cooling to room temperature, pyridine was evaporated under reduced pressure. The semisolid residue was dissolved in a mixture of 50 mL of water and 50 mL of methylene chloride with vigorous mixing. The organic layer was separated and washed with water. The evaporation of the solvent left 3.0 g of the crude oxime as a thick colorless oil. A portion (2.5 g, 10 mmol) of the thick oil was dissolved in 50 mL of pyridine, and 2.7 g (14 mmol) of tosyl chloride was added in one portion. The mixture was heated to reflux for 1 h and then cooled to room temperature. Pyridine was evaporated at reduced pressure. A mixture of 50 mL of water and 50 mL of methylene chloride was added to the semisolid residue and mixed well. The organic layer was separated and washed with water, 1 N aqueous HCl, and water. The solvent was evaporated under reduced pressure to leave 4.38 g of colorless semisolid crude oxime-tosylate. This was

https://dx.doi.org/10.1021/acschemneuro.0c00667
ACS Chem. Neurosci. 2021, 12, 176−183

dissolved in 20 mL of methylene chloride in a 100 mL round-bottom flask equipped with a magnetic stir bar and a dry ice/acetone cold bath. A dry ice cooled gas condenser was attached, and 20 mL of liquid ammonia was condensed into the flask. The cold bath was removed, and the mixture was stirred under the dry ice/acetone filled gas condenser for several hours. Then, the condenser was allowed to warm, and the ammonia was allowed to evaporate from the solution overnight. In the morning, a mixture of 50 mL of water and 50 mL of methylene chloride was added. The organic layer was removed and was washed with water and then evaporated under reduced pressure. The semisolid residue was triturated with 50 mL of hexane. Evaporation of the hexane left 2.5 g of semisolid crude diaziridine. A 100 mL round-bottom flask with magnetic stir bar was filled with 1.40 g (5.65 mmol) of the crude diaziridine, 60 mL of methylene chloride, and 3.5 mL of triethylamine. The stirred solution was cooled in an ice bath. Iodine (1.45 g, 5.70 mmol) was added in one portion. The mixture was stirred in the ice bath until the solid iodine dissolved; then, it was allowed to warm to room temperature and to stir for 1 h. A solution of 1 N potassium hydroxide (30 mL) was added, and the mixture was vigorously stirred for 30 min. Water (100 mL) was added, and the mixture was extracted with methylene chloride (3 × 30 mL). The combined organic extracts were washed with 100 mL of 1 M aqueous HCl solution and 100 mL of water and then dried. The evaporation of the solvent left 1.3 g of brown oil. The residue was dissolved in hexane and flushed through a short plug of silica gel using additional hexane as eluent. The evaporation left a clear colorless oil that was dynamically transferred under high vacuum to a liquid nitrogen cooled U-trap to give 1.0 g (72%) of a very pale pink liquid. The product was greater than 98% pure when analyzed by capillary GC (30 m dimethylsilicone column, 150 °C injector, 100 °C column temp). ^{1}H NMR (500 MHz, $CDCl_3$) 7.35 (t, J = 7.0 Hz, 1H), 7.30 (t, J = 7.0 Hz, 1H), 7.13 (t, J = 7.8 Hz), 3.27 (septet, J = 7 Hz, 1H), 1.25 ppm (d, J = 7 Hz, 6H). ^{19}F-NMR (340 MHz, $CDCl_3$) −68.65 (d, J = 7.8 Hz, 3F), −119.40 ppm (td, J = 7.8, 7.0 Hz, 1F). ^{13}C NMR (90 MHz, $CDCl_3$) 160.2 (d, J = 252 Hz), 136.8 (d, J = 15 Hz), 130.0 (d, J = 5 Hz), 127.9 (d, J = 2 Hz), 124.7 (d, J = 5 Hz), 121.8 (q, J = 275 Hz), 115.5 (d, J = 16 Hz), 27.0 (d, J = 2 Hz), 25.6 (q, J = 43 Hz), 22.5 ppm. HRMS(EI+) calculated for $C_{11}H_{11}F_4N_2$ $[M + H]^+$: 247.0858, found: 247.0869.

Physicochemical Properties of AziFo. Octanol/water partition coefficients were calculated using XLOGP3.[23] Molecular volume was calculated using the Molinspiration property calculation toolkit (Molinspiration Cheminformatics). The density of fropofol was determined from replicate measurements of the volume/mass relationship. The measurement of the UV−vis absorbance (Varian Cary 300 Bio UV−vis spectrophotometer) of AziFo showed a maximum diazirine absorbance at 317 nm with additional aromatic absorption maxima at 267 and 273 nm. The extinction coefficient (Σ_{273} = 1600 M^{-1} cm^{-1}) was calculated from UV absorption measurements from the aromatic absorption at 273 nm in methanolic solutions of known concentrations. The extinction coefficient was used to calculate the maximal water solubility of AziFo after 24 h of sonication in double distilled water (ddH_2O) and filtration with a 0.22 μm polyvinylidene difluoride (PVDF) syringe (MidSci, St. Louis, MO).

1-Aminoanthracene Competition Fluorescence Assay. This assay was performed in a similar manner to that previously described with a few modifications.[7,13,24] A saturated solution of 1-AMA (1-aminoanthracene, Sigma-Aldrich, technical grade) was prepared by sonication in Dulbecco's phosphate buffered saline (DPBS, pH = 7.4) followed by filtration with a 1.2 μm glass microfiber filter (Whatman). The concentration was determined by UV−vis spectroscopy utilizing an experimentally determined extinction coefficient of 1-AMA (Σ_{368} = 4073 M^{-1} cm^{-1}; see Figure S8). Stock solutions of ligand (AziFo or fropofol) were prepared in DMSO due to limited aqueous solubility. Horse spleen apoferritin (HSAF, Sigma-Aldrich, 0.2 μm filtered) was used as received. 1-AMA (15 μM final concentration) was pre-equilibrated with HSAF (15 μM dimer final concentration), and 5 μL of ligand stock in DMSO was then added for a final volume of 500 μL (1% DMSO v/v in DPBS) with the final ligand concentrations ranging from 1 to 125 μM. Upon addition of the ligand, the samples were mixed and immediately analyzed with a spectrofluorometer (Shimadzu RF-5301 PC) with an excitation wavelength of 380 nm and emission detection from 400 to 700 nm. The fluorescence curves were corrected by subtracting contributions from 1-AMA alone and HSAF alone. There was no significant fluorescent signal from unbound ligands. Fluorescence intensities at 515 nm were plotted as a percentage of the control (1-AMA and HSAF bound with no competing ligand present) and were fitted to a logarithmic four parameter variable slope using GraphPad Prism (version 8.4.0, GraphPad Software, La Jolla California, USA). This experimentally determined IC_{50} was used to calculate the dissociation constant via an experimentally determined K_D of 1-AMA and the Cheng-Prusoff equation.[18]

Activity in Zebrafish. All zebrafish were treated in strict accordance with NIH and institutional guidelines, and procedures were approved by the University of Pennsylvania Animal Care and Use Committee and conducted in accordance with the Guide for Care and Use of Laboratory Animals. Adult Tübingen long fin wild-type zebrafish (*Danio rerio*) were maintained at the University of Pennsylvania's aquatic facility and overseen by the University Laboratory Animal Resources using standard husbandry conditions. In vivo behavioral activity studies were performed on zebrafish at 5 days postfertilization (dpf). Zebrafish embryos were raised in E3 zebrafish embryo water (5 mM NaCl, 0.17 mM KCl, 0.33 mM $CaCl_2$, 0.33 mM $MgSO_4$, pH 7.2) at 28.5 °C in a 14:10 h light/dark cycle. Each replicate consisted of 12 larvae. At least three independent biological replicates for dosage were derived from different clutches of embryos and were recorded on different days. Because no decrease in spontaneous movement was observed with any AziFo or fropofol concentration, these ligands were coadministered with propofol to evaluate pharmacological additivity. Each sample well contained 2 mL of E3 with various concentrations of AziFo or fropofol (0, 5, or 25 μM) and propofol (0.003−30 μM, Aldrich, 97%). Stock solutions of drug were made in DMSO and diluted in E3. The final concentration of DMSO (Sigma, sterile-filtered, BioReagent) was always below 2% v/v, which showed no signs of toxicity or change in the measured movement parameters. Larvae were acclimatized to the 24-well plates (1 fish/well) for approximately 20 min in E3 at 25 °C prior to ligand exposure. The solution was removed from each well and replaced with 2 mL of E3 with drug for a total of 30 min. Infrared video recordings were made using a Daniovision Observation Chamber (Noldus). The recordings were analyzed for spontaneous propulsive movements (total distance moved) for the final 10 min of the 30 min exposure. After drug exposure, the drug solution in each well was replaced with fresh E3, and the zebrafish were kept for observation over the next 24 h and monitored for signs of toxicity and spontaneous recovery in anesthetized groups. At 24 h, all zebrafish were euthanized by submersion in ice water for at least 20 min.

AziFo Diazirine Half-Life. The rate of photolysis of the AziFo diazirine was determined in methanol in a 1 cm path length quartz cuvette exposed to 300 and 350 nm UV light (Rayonet RPR-3500 lamp) at a distance from the light source of approximately 1 cm. The half-life was unable to be determined in aqueous solution due to limitations of solubility and the ability to detect the absorption of the diazirine peak. The disappearance of the diazirine absorption peak was monitored via serial UV−vis measurements.

Photolabeling HSAF with AziFo. Solutions containing 50 μg (1 mg/mL, 25 μM dimer) of HSAF (Sigma-Aldrich, 0.2 m filtered) were equilibrated with 10 or 100 μM AziFo in DPBS (pH = 7.4) for 25 min on ice in the dark. AziFo stock solutions were prepared in DMSO for a final concentration of 1% DMSO (v/v). The samples were transferred to 1 mm path length quartz cuvettes and exposed to a 300 nm light (Rayonet RPR-3500 lamp) for a total of 25 min. Proteins were then precipitated with acetone, resuspended in buffer, reduced with dithiothreitol, and alkylated with iodoacetamide and underwent in-solution protease digestion with trypsin. Samples were desalted with C18 stage tips in preparation for LC/MS/MS analysis.[25] Digested protein preparations were analyzed by an Orbitrap Elite Hybrid Ion Trap-Orbitrap Mass Spectrometer (MS) coupled to an

https://dx.doi.org/10.1021/acschemneuro.0c00667
ACS Chem. Neurosci. 2021, 12, 176−183

Easy-nanoLC 1000 system. Spectral analysis was conducted using MaxQuant (Max Planck Institute of Biochemistry).[26] For more detailed methods, see the Supporting Information.

Molecular Docking Calculations. The calculations of ligand docking poses were generated using a previously published crystal structure of HSAF (PDB ID 3f32, 1.7 Å resolution).[21] From the molecular assembly, a homodimer was generated, and small molecules (water and sulfate and cadmium ions) were removed with PyMOL (The PyMOL Molecular Graphics System, Version 2.3.5 Schrödinger, LLC.). AutoDock Tools was used to add Gasteiger charges and merge nonpolar hydrogens.[27] The 2D drawing and 3D optimization of the ligand structures were performed in ChemDoodle (version 9.1.0, iChemLabs) followed by conversion to .pdbqt files with PyMOL and AutoDock Tools. Maximum torsions were added to each ligand to allow full flexibility. Ligand docking was conducted with AutoDock Vina with an 18 × 20 × 20 Å grid box centered at the homodimer interface.[22,27] All default algorithmic parameters were used including side chain flexibility and exhaustiveness. Images and atomic measurements were generated with PyMOL. The identification of atoms lining the solvent accessible pocket was conducted with CASTp.[28]

■ ASSOCIATED CONTENT

Supporting Information

The Supporting Information is available free of charge at https://pubs.acs.org/doi/10.1021/acschemneuro.0c00667.

NMR, absorbance, fluorescence, and MS/MS spectra with associated ion fragmentation tables, HSAF sequence coverage, CASTp analysis, an additional table of docking simulation data, and supplemental methods (PDF)

■ AUTHOR INFORMATION

Corresponding Author

Roderic G. Eckenhoff − *Perelman School of Medicine, Department of Anesthesiology and Critical Care, University of Pennsylvania, Philadelphia, Pennsylvania 19104, United States*; Phone: 215-662-3705; Email: roderic.eckenhoff@pennmedicine.upenn.edu; Fax: 215-349-5078

Authors

E. Railey White − *Perelman School of Medicine, Department of Anesthesiology and Critical Care, University of Pennsylvania, Philadelphia, Pennsylvania 19104, United States*; orcid.org/0000-0001-9729-6394

David M. Leace − *Perelman School of Medicine, Department of Anesthesiology and Critical Care, University of Pennsylvania, Philadelphia, Pennsylvania 19104, United States*

Victoria M. Bedell − *Perelman School of Medicine, Department of Anesthesiology and Critical Care, University of Pennsylvania, Philadelphia, Pennsylvania 19104, United States*

Natarajan V. Bhanu − *Perelman School of Medicine, Department of Biochemistry and Biophysics, Smilow Center for Translational Research, University of Pennsylvania, Philadelphia, Pennsylvania 19104, United States*

Benjamin A. Garcia − *Perelman School of Medicine, Department of Biochemistry and Biophysics, Smilow Center for Translational Research, University of Pennsylvania, Philadelphia, Pennsylvania 19104, United States*; orcid.org/0000-0002-2306-1207

William P. Dailey − *Department of Chemistry, University of Pennsylvania, Philadelphia, Pennsylvania 19104, United States*

Complete contact information is available at: https://pubs.acs.org/10.1021/acschemneuro.0c00667

Author Contributions

R.G.E. and W.P.D. conceived the original idea. E.R.W. directed the project with supervision from R.G.E. W.P.D. performed all chemical syntheses and characterizations. N.V.B. analyzed the MS/MS samples under the supervision of B.A.G. V.M.B. performed the zebrafish experiments. E.R.W. and D.M.L. performed all the remaining experiments and took the lead in writing the manuscript with input from all the authors who provided critical feedback and helped shape the research, analysis, and manuscript.

Funding

This work was funded by the following sources: Research Fellowship Grant from the Foundation for Anesthesia Education and Research, National Institutes of Health National Institute of General Medical Sciences grants P01-GM-055876, R01-GM-110174, and T32-GM-112596.

Notes

The authors declare no competing financial interest.

■ ACKNOWLEDGMENTS

The authors would like to thank Dr. Michael A. Pack (University of Pennsylvania, Perelman School of Medicine, Department of Medicine) for graciously providing wild-type zebrafish larvae.

■ ABBREVIATIONS

1-AMA, 1-aminoanthracene; AziF*o*, *ortho*-azi-fropofol; AziP*m*, *meta*-Azi-propofol; $CDCl_3$, deuterated chloroform; CI, confidence interval; cLogP, octanol/water partition coefficient; E3, E3 zebrafish embryo water; HCl, hydrochloric acid; HCM, hypertrophic cardiomyopathy; HSAF, horse spleen apoferritin; dpf, days postfertilization; DPBS, Dubelco's phosphate buffered saline; HRMS, high resolution mass spectrometry; PAL, photoaffinity label; PFTBA, perfluorotributylamine; PVDF, polyvinyl difluoride; *sec*-BuLi, *sec*-butyllithium; $t_{1/2}$, half-life

■ REFERENCES

(1) White, P. F., and Warner, D. S. (2008) Propofol: Its Role in Changing the Practice of Anesthesia. *Anesthesiology 109* (6), 1132−1136.

(2) Feng, A. Y., Kaye, A. D., Kaye, R. J., Belani, K., and Urman, R. D. (2017) Novel Propofol Derivatives and Implications for Anesthesia Practice. *J. Anaesthesiol. Clin. Pharmacol. 33* (1), 9−15.

(3) Brosnan, R. J., and Pham, T. L. (2016) GABAA Receptor Modulation by Phenyl Ring Compounds Is Associated with a Water Solubility Cut-Off Value. *Pharmacology 98* (1−2), 13−19.

(4) James, R., and Glen, J. B. (1980) Synthesis, Biological Evaluation, and Preliminary Structure-Activity Considerations of a Series of Alkylphenols as Intravenous Anesthetic Agents. *J. Med. Chem. 23* (12), 1350−1357.

(5) Krasowski, M. D., Jenkins, A., Flood, P., Kung, A. Y., Hopfinger, A. J., and Harrison, N. L. (2001) General Anesthetic Potencies of a Series of Propofol Analogs Correlate with Potency for Potentiation of Gamma-Aminobutyric Acid (GABA) Current at the GABA(A) Receptor but Not with Lipid Solubility. *J. Pharmacol. Exp. Ther. 297* (1), 338−351.

(6) Trapani, G., Latrofa, A., Franco, M., Altomare, C., Sanna, E., Usala, M., Biggio, G., and Liso, G. (1998) Propofol Analogues. Synthesis, Relationships between Structure and Affinity at GABA(A) Receptor in Rat Brain, and Differential Electrophysiological Profile at

Recombinant Human GABA(A) Receptors. *J. Med. Chem. 41* (11), 1846−1854.
(7) Woll, K. A., Weiser, B. P., Liang, Q., Meng, T., McKinstry-Wu, A., Pinch, B., Dailey, W. P., Gao, W. D., Covarrubias, M., and Eckenhoff, R. G. (2015) Role for the Propofol Hydroxyl in Anesthetic Protein Target Molecular Recognition. *ACS Chem. Neurosci. 6* (6), 927−935.
(8) Dimitrov, I. V., and Suonio, E. E. K. (2020) Syntheses of Analogues of Propofol: A Review. *Synthesis 52* (24), 3693−3713.
(9) Eckenhoff, R., and Tang, P. (2018) Recent Progress on the Molecular Pharmacology of Propofol. *F1000Research 7*, 123.
(10) Woll, K. A., Dailey, W. P., Brannigan, G., and Eckenhoff, R. G. (2016) Shedding Light on Anesthetic Mechanisms: Application of Photoaffinity Ligands. *Anesth. Analg. 123* (5), 1253−1262.
(11) Ge, S. S., Chen, B., Wu, Y. Y., Long, Q. S., Zhao, Y. L., Wang, P. Y., and Yang, S. (2018) Current Advances of Carbene-Mediated Photoaffinity Labeling in Medicinal Chemistry. *RSC Adv. 8* (51), 29428−29454.
(12) Murale, D. P., Hong, S. C., Haque, M. M., and Lee, J. S. (2016) Photo-Affinity Labeling (PAL) in Chemical Proteomics: A Handy Tool to Investigate Protein-Protein Interactions (PPIs). *Proteome Sci. 15* (1), 14.
(13) Hall, M. A., Xi, J., Lor, C., Dai, S., Pearce, R., Dailey, W. P., and Eckenhoff, R. G. (2010) M-Azipropofol (AziPm) a Photoactive Analogue of the Intravenous General Anesthetic Propofol. *J. Med. Chem. 53* (15), 5667−5675.
(14) Yip, G. M. S., Chen, Z. W., Edge, C. J., Smith, E. H., Dickinson, R., Hohenester, E., Townsend, R. R., Fuchs, K., Sieghart, W., Evers, A. S., and Franks, N. P. (2013) A Propofol Binding Site on Mammalian GABA A Receptors Identified by Photolabeling. *Nat. Chem. Biol. 9* (11), 715−720.
(15) Colard, J. N., Hornsperger, J. M., and Schirlin, D. (1994) *Aromatic Acetylcholinesterase Inhibitors*. EP 0627400 A1.
(16) Wang, L., Yoshida, T., Muto, Y., Murai, Y., Tachrim, Z. P., Ishida, A., Nakagawa, S., Sakihama, Y., Hashidoko, Y., Masuda, K., Hatanaka, Y., and Hashimoto, M. (2015) Synthesis of Diazirine-Based Photoreactive Saccharin Derivatives for the Photoaffinity Labeling of Gustatory Receptors. *Eur. J. Org. Chem. 2015* (14), 3129−3134.
(17) DiMagno, S., and Sun, H. (2006) The Strength of Weak Interactions: Aromatic Fluorine in Drug Design. *Curr. Top. Med. Chem. 6* (14), 1473−1482.
(18) Lazareno, S., and Birdsall, N. J. M. (1993) Estimation of Competitive Antagonist Affinity from Functional Inhibition Curves Using the Gaddum, Schild and Cheng-Prusoíf Equations. *Br. J. Pharmacol. 109* (4), 1110−1119.
(19) Bedell, V. M., Meng, Q. C., Pack, M. A., and Eckenhoff, R. G. (2020) A Vertebrate Model to Reveal Neural Substrates Underlying the Transitions between Conscious and Unconscious States. *Sci. Rep. 10* (1), 15789.
(20) Qiu, L., Lin, J., Liu, Q., Wang, S., Lv, G., Li, K., Shi, H., Huang, Z., and Bertaccini, E. J. (2017) The Role of the Hydroxyl Group in Propofol-Protein Target Recognition: Insights from ONIOM Studies. *J. Phys. Chem. B 121* (24), 5883−5896.
(21) Vedula, L. S., Brannigan, G., Economou, N. J., Xi, J., Hall, M. A., Liu, R., Rossi, M. J., Dailey, W. P., Grasty, K. C., Klein, M. L., Eckenhoff, R. G., and Loll, P. J. (2009) A Unitary Anesthetic Binding Site at High Resolution. *J. Biol. Chem. 284* (36), 24176−24184.
(22) Trott, O., and Olson, A. J. (2010) Software News and Update Auto Dock Vina: Improving the Speed and Accuracy of Docking with a New Scoring Function, Efficient Optimization, and Multithreading. *J. Comput. Chem. 31* (2), 455−461.
(23) Cheng, T., Zhao, Y., Li, X., Lin, F., Xu, Y., Zhang, X., Li, Y., Wang, R., and Lai, L. (2007) Computation of Octanol-Water Partition Coefficients by Guiding an Additive Model with Knowledge. *J. Chem. Inf. Model. 47* (6), 2140−2148.
(24) Butts, C. A., Xi, J., Brannigan, G., Saad, A. A., Venkatachalan, S. P., Pearce, R. A., Klein, M. L., Eckenhoff, R. G., and Dmochowski, I. J. (2009) Identification of a Fluorescent General Anesthetic, 1-Aminoanthracene. *Proc. Natl. Acad. Sci. U. S. A. 106* (16), 6501−6506.
(25) Rappsilber, J., Mann, M., and Ishihama, Y. (2007) Protocol for Micro-Purification, Enrichment, Pre-Fractionation and Storage of Peptides for Proteomics Using StageTips. *Nat. Protoc. 2* (8), 1896−1906.
(26) Tyanova, S., Temu, T., and Cox, J. (2016) The Max Quant Computational Platform for Mass Spectrometry-Based Shotgun Proteomics. *Nat. Protoc. 11* (12), 2301−2319.
(27) Morris, G. M., Huey, R., Lindstrom, W., Sanner, M. F., Belew, R. K., Goodsell, D. S., and Olson, A. J. (2009) AutoDock4 and AutoDock Tools4: Automated Docking with Selective Receptor Flexibility. *J. Comput. Chem. 30* (16), 2785−2791.
(28) Tian, W., Chen, C., Lei, X., Zhao, J., and Liang, J. (2018) CASTp 3.0: Computed Atlas of Surface Topography of Proteins. *Nucleic Acids Res. 46* (W1), W363−W367.

https://dx.doi.org/10.1021/acschemneuro.0c00667
ACS Chem. Neurosci. 2021, 12, 176−183